Coastal Engineering 184 (2023) 104340

Contents lists available at ScienceDirect

Coastal Engineering

journal homepage: www.elsevier.com/locate/coastaleng

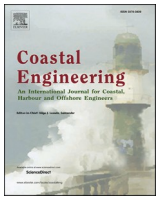

Experimental study on the morphodynamic evolution of sandbar-lagoon system with emergent vegetation

Xin Cong [a], Cuiping Kuang [a,*], Guangwei Huang [a], Qingping Zou [b,**], Xuejian Han [a], Chao Shen [a], Jie Gu [c]

[a] College of Civil Engineering, Tongji University, Shanghai, 200092, China
[b] The Lyell Centre for Earth and Marine Science and Technology, Institute for Infrastructure and Environment, Heriot-Watt University, Edinburgh, EH14 4AS, UK
[c] College of Marine Ecology and Environment, Shanghai Ocean University, Shanghai, 201306, China

ARTICLE INFO

Keywords:
Vegetation density
Sandbar-lagoon system
Dune erosion
Wave attenuation

ABSTRACT

A mobile-bed sandbar-lagoon model was employed in a series of flume experiments to investigate the influence of vegetation with different densities over the sandbar on wave attenuation and bed profile evolution. Nineteen flume tests were carried out for the same sandbar-lagoon model under different conditions. Extensive analyses were conducted on the profile evolution and the wave parameters along the profile of the sandbar-lagoon system. Based on the weighted vegetation density by the canopy width, a new empirical relationship was established between wave attenuation and vegetation density, water depth and sandbar freeboard. It was found that wave attenuation increases with the rise of sandbar freeboard and weighted vegetation density, and decreases with the fall of incident wave height. The collision (s-shaped scarp) and overwash (upward concave scarp) types of fore-dune morphological evolution were observed in the experiments. The maximum erosion thickness of dune follows a quadratic polynomial relationship with vegetation density, indicating that too sparse vegetation cover may lead to more erosion. It follows that an optimal vegetation density may lead to the least wave reflection due to the quadratic polynomial relationship. However, when the maximum erosion thickness of fore-dune is small, the quadratic polynomial relationship becomes linear. Furthermore, the experimental results indicate that wave height, water depth, sandbar freeboard and vegetation density are all important contributing factors to the morphodynamic evolution of sandbar-lagoon system with emergent vegetation. These relationships promote the development of wave-vegetation-sediment mechanics and provide a scientific guide to carry out coastal ecological restoration projects, especially in the sandbar-lagoon system.

1. Introduction

Coastal biome accounted for more than 37% in the global ecosystem services with an estimated value of US$12.6 trillion per year (Costanza et al., 1997). Coastal lagoons and wetlands cover 13% of coastlines and represent one of the most valuable ecosystems which support nearly 40% of the population within 100 km of coasts (Clara et al., 2017; Suresh et al., 2021). However, lagoons and wetlands are threatened by economic developments along the coast, and climate changes including rising sea levels and increased storm amplitude and frequency (Hanley et al., 2020). Coastal vegetation is a natural sea defense at a fraction of the cost of hard defenses such as seawalls and breakwaters (Kirwan and Megonigal, 2013; Morris et al., 2018), and is critical in maintaining a healthy ecological system. With growing interest in coastal resilience, vegetation canopy has become a popular nature-based solution for ecological restoration, sea dike reinforcement (Ponsioen et al., 2019; Pan et al., 2018), sand trapping and wind break (Fu et al., 2021; Li et al., 2022a).

Vegetation has a significant wave attenuation capability and higher density and biomass lead to greater wave attenuation (Möller et al., 2011, 2014; Maza et al., 2015). In the past decade, extensive laboratory studies have been dedicated to better understanding the wave attenuation by rigid and flexible vegetation (Lowe et al., 2005; Augustin et al., 2009; Stratigaki et al., 2011; Manca et al., 2012; Koftis et al., 2013; Ozeren et al., 2014; Anderson and Smith, 2014; Wu and Cox, 2015; Paul et al., 2012; Luhar et al., 2017; Yin et al., 2020). Anderson and Smith

* Corresponding author.
** Corresponding author.
E-mail addresses: cpkuang@tongji.edu.cn (C. Kuang), q.zou@hw.ac.uk (Q. Zou).

https://doi.org/10.1016/j.coastaleng.2023.104340
Received 11 June 2022; Received in revised form 21 March 2023; Accepted 26 May 2023
Available online 2 June 2023

(2014) proposed that stem density and the ratio of stem length to water depth are the key factors in wave attenuation of single- and double-peaked irregular waves. Lei and Nepf (2019) characterized the impact of artificial flexible plants reconfiguration on wave decay by an effective blade length and liked individual blade dynamics to meadow scale. Experiments in one of the largest wave flumes in the world (Rupprecht et al., 2017) showed that plant flexibility and height, wave condition and water depth are determining factors for salt marsh vegetation interactions with waves. Türker et al. (2019) used model cylinders composed of dried *phragmites australis* stems and found high correlation between wave damping and non-dimensional vegetated length parameter.

Dalrymple et al. (1984) and Kobayashi et al. (1993) established theoretical models for the wave attenuation by submerged and emergent rigid canopies. Zhu and Zou (2017) generalized an analytical solution, indicating that wave attenuation increases with the rising elevation of the suspended vegetation canopy from the bottom and the rise of incident wave height and wave period. Zhu et al. (2020) developed analytical solutions for random wave attenuation of submerged and suspended flexible vegetation canopy that reduce to the solutions by Mendez and Losada (2004), Chen and Zhao (2012) and Jacobsen et al. (2019) for submerged rigid aquatic vegetation and verified aquaculture farms as nature-based coastal protection. Chen and Zou (2019) combined an OpenFOAM (Higuera et al., 2013) hydrodynamics model with an immersed element model of flexible vegetation and observed a strong jet at the top of a submerged canopy opposite to wave direction. Zhang et al. (2021b) developed a simple wave damping model for flexible marsh plants considering sheltering effect. Zhao et al. (2023) obtained a linear relationship between the wave transmission coefficient and a new parameter dependent on the Iribarren number, relative water depth, vegetation width, submergence, and vegetation density based on experiments. Maza et al. (2022) related wave damping to the hydraulic standing biomass containing the meadow mean height, standing biomass and incident flow characteristics.

Vegetation can reduce dune erosion effectively and it is directly connected with the energy dissipation depending on vegetation cover (Figlus et al., 2017; Ayat and Kobayashi, 2015). Localized energy dissipation by vegetation creates a shadow region of low wave energy, which may have important implications for neighboring coastal area (Dalrymple et al., 1984). Based on the rate of energy change for dislocating sediment particles proposed by Türker and Kabdasli (2004), a linear correlation was depicted (Türker et al., 2019) between wave energy dissipation by vegetation cover and energy to erode the coastal dune. To capture a range of morphodynamic responses to storms, Sallenger (2000) proposed four storm impact regimes (swash, collision, overwash and inundation), which has been adopted as a measure of storm impacts on coastlines (Jackson and Short, 2020; Han et al., 2022). According to the morphodynamic transition time between two neighboring storm impact regimes, Odériz et al. (2020) used internal rock core structure to strengthen the dune, and studied the effects of vegetation positions under storm conditions. It was found that the vegetation provides a better protection in the initial swash and collision regimes, while the rock core is better preventing overwash and dune destruction during the final stages of storm impacts.

In addition, the evolution of artificial sandbar or submerged berms has attracted lots of attention recently due to its complexity and significance. Pan et al. (2022, 2023) conducted a series of flume experiments to investigate the evolution of a submerged berm under regular and irregular waves in low-energy conditions. There is a lack of experimental study on coastal profile evolution in the presence of vegetation canopy (Silva et al., 2016; Astudillo et al., 2022). Even fewer studies have been reported on the vegetated sandbar-lagoon system. Unlike previous studies on wave and beach profile changes with emergent vegetation of bamboo stick (Kuang et al., 2021), real aquatic plants of *dracaena sanderiana* (Cong et al., 2021a), and submerged vegetation made of optical fiber (Cong et al., 2021b, 2022), this study investigates the morphodynamic evolution of a sandbar-lagoon system with emergent aquatic vegetation during storms. It is structured as follows: Section 2 is concentrated on experimental set-up and data analysis, Section 3 presents the results, Section 4 focuses on the discussion, and Section 5 concludes the main point of the study.

2. Methods

2.1. Experimental setup

The mobile-bed experiment was carried out in a 50 m long × 0.8 m wide × 1.2 m deep wave flume in the Laboratory of Hydraulic and Harbor Engineering, Tongji University. The experimental layout was shown in Fig. 1 and the photos of experiment layout were presented in Fig. 2. This study focused on an eroded sandy lagoon coast system without beach shoulder and with only fore-dune face. The sandbar crest was 1 m long and 0.48 m high, and all slopes were set as 1:2. The back side of the coastal fore-dune was supported by a 0.8 m high polypropylene (PP) board. Wave data were collected by seven capacitive wave gauges (W1–W7) and four acoustic wave gauges (Wa~Wd), all with a sampling frequency of 50 Hz. The wave gauge locations were marked in Fig. 1. The entire experiment process was recorded by three Signal Lens Reflex (SLR) cameras installed near the sandbar, lagoon and coastal fore-dune, respectively. The following coordinate system was adopted (Fig. 1): the horizontal axis $x = 0$ is at the location of W1; the vertical axis $z = 0$ is at the bottom of the flume.

Emergent vegetation was mimicked by bamboo sticks with a diameter of 4 mm, and the vegetation canopy was 0.50 m long at the sandbar crest and 0.24 m long at the front slope of the sandbar (as shown in Fig. 1). Vegetation was planted according to the rectangular distribution with two kinds of density (see Fig. 3 for the vegetation configuration). The vegetation density was reduced by removing some rows in the wave direction. Bamboo sticks were fixed in a prefabricated PP board (Fig. 4a) placed in the bottom of the bar (Fig. 4b) with enough freeboard (Fig. 1). The specific experimental procedure was as follows. Pre-buried pits were laid in the area where vegetation needs to be arranged on the moving bed; prefabricated planter plates were for simulating emergent plant planting; emergent plants were simulated on the planter plate. Planting plates with emergent plants were placed in a pre-buried pit; the backfill sand was filled layer by layer in the pre-buried pit. After each layer of backfill sand was filled, water injection and vibration operation were carried out for the backfill sand in the pre-buried pit until the filling height of the pre-buried pit was consistent with the height of the moving bed. The plant distribution density ϕ was calculated using the formula by Tanino and Nepf (2008).

$$\phi = \frac{V_s}{V} = \frac{N \times S_i}{S} \tag{1}$$

where V_s is the submerged volume of vegetation; V is the total volume of water column occupied by the plant canopy. In this experiment, volume can be converted into area to calculate the distribution density of emergent vegetation. N is the total number of plants in the coverage area; S_i is the cross-sectional area of a single plant ($S_i = \pi r_v^2$, r_v is the radius of a single plant); S is the total area covered by vegetation canopy.

The vegetation distribution density was calculated using the above method on the sea-side slope and the sandbar crest, respectively. However, vegetation canopy width in the direction of wave propagation (Fig. 3b) also has a significant effect on wave attenuation and dune erosion. The vegetation width was considered in the weighted density ϕ_w, resulting in a dimension of 'meter' using the following formula.

$$\phi_w = a_1\phi_1 + a_2\phi_2 \tag{2}$$

where a_1 and a_2 are the vegetation canopy width (Fig. 3b) on the sea-side slope and the sandbar crest, respectively; ϕ_1 and ϕ_2 are the corresponding vegetation density, respectively.

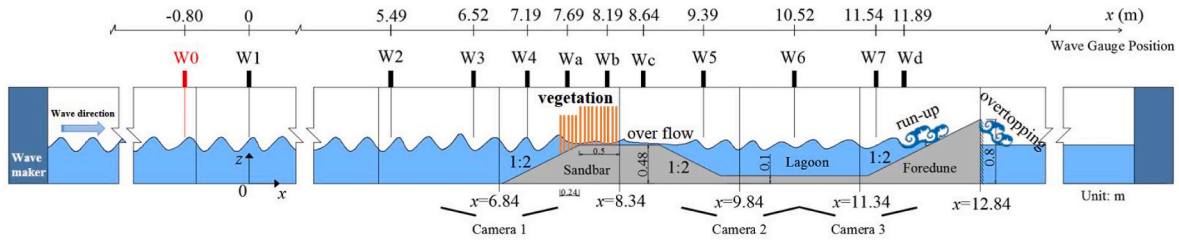

Fig. 1. Experimental setup diagram for a sandbar-lagoon system with emergent vegetation in a 50 m long × 0.8 m wide × 1.2 m deep wave flume. Wave data was collected by seven capacitive wave gauges (W1–W7) and four acoustic wave gauges (Wa~Wd).

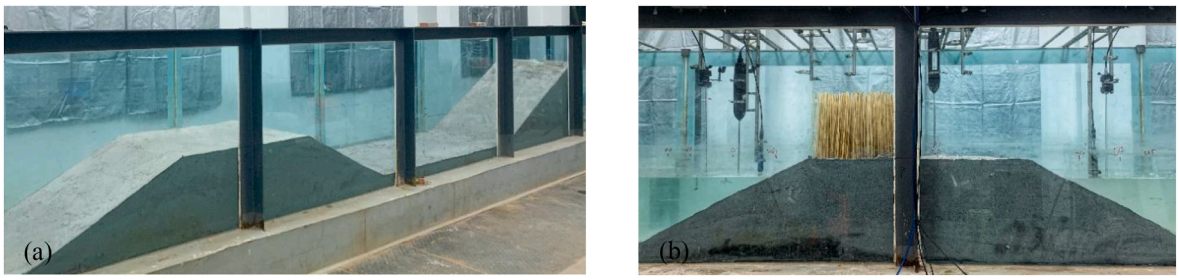

Fig. 2. Experiemental layout of (a) sandbar-lagoon-foredune system and (b) vegetation canopy at the crest of sand bar.

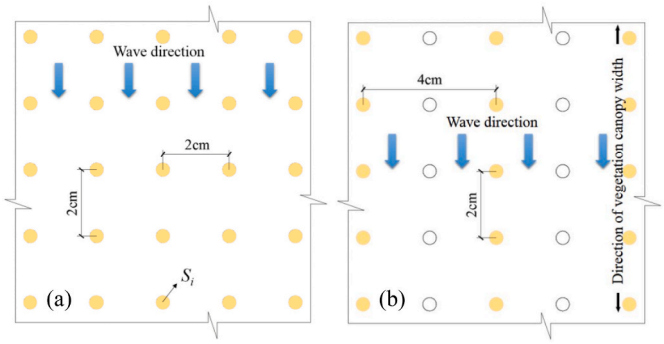

Fig. 3. Top view of vegetation canopy in rectangular distribution with (a) high and (b) low density. Yellow and empty circles indicate the locations with and without vegetation attached to the prefabricated PP board.

Wave data collected at the Qilihai buoy station in Qinhuangdao city from April to December 2019 was used as the incident waves. The model scale 1:10 was designed following (Yin et al., 2017; Ma et al., 2020; Kuang et al., 2020) and detailed steps can be found in **Appendix**. Two water depths (d) of 0.48 m and 0.55 m were taken into consideration in this experiment. The incident significant wave height, vegetation density, and weighted vegetation density were shown in Table 1. For d = 0.48 m, seven test conditions were designed; for d = 0.55 m, twelve test conditions were implemented. The irregular wave generated by JONSWAP spectrum was used in the experiment. The measured spectra obtained in the empty flume by the capacitive wave gauge located at W0 was shown in Fig. 5.

2.2. Data analysis

In this study, all data analysis was carried out using MATLAB R2019b. Significant wave height $H_{1/3}$ was obtained using the relationship between statistical characteristics of wave surface elevation and wave spectra. 8192 sampling points with a sampling frequency of 0.02 s were used for each test, and each test lasts 2.73 min. First, wave time-series data were standardized: time series of raw data A minus time series after the moving mean function $movmean$ (A, k), where the parameter value k of the sliding window length was taken as the sampling points contained in a wave period. Then, wave spectra were obtained through the fast Fourier transform method. Finally, the significant wave height was calculated using $H_{1/3} = 4m_0^{1/2}$, where m_0 is the zero-order moment of the wave spectrum. The wave reflection coefficient was calculated by separating the incident and reflected wave heights based on the wave data at W2 and W3 wave gauge, following Goda and Suzuki (1976). According to the incident wave amplitude a_i

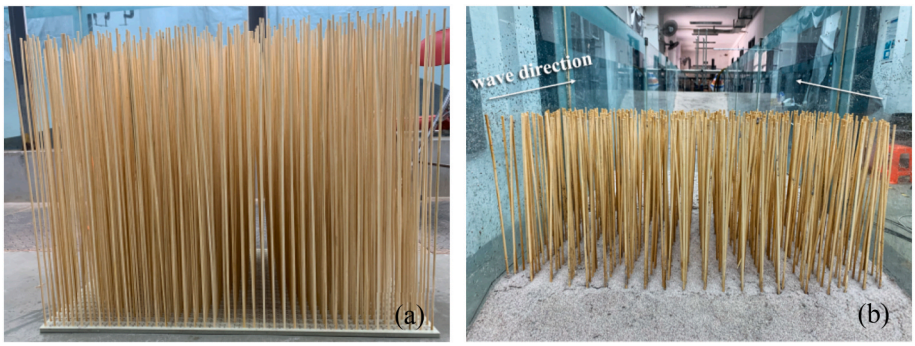

Fig. 4. Mimicked vegetation canopy with bamboo sticks. (a) Vegetation attached to a prefabricated PP board; (b) Vegetation layout over a sandbar crest before erosion occurs.

Table 1
Parameters of Physical experimental tests. H_0 and T_0 is the incident significant wave height and wave period; ϕ and ϕ_w is the non-weighted and weighted vegetation density. Test names are denoted by **L**: **L**ow water depth; **H1**: **H**igh water depth with H_0 of **0.16m**; **H2**: **H**igh water depth with H_0 of **0.21m**; **N**: **N**o vegetation; **CH**: Bar **C**rest with vegetation of **H**igh density; **SH**: Bar fore **S**lope with vegetation of **H**igh density; **CL**: Bar **C**rest with vegetation of **L**ow density; **SL**: Bar fore **S**lope with vegetation of **L**ow density.

Test name				H_0 (m)		T_0 (s)		ϕ (−)		ϕ_w (m)
Water depth d = 0.48 m		Water depth d = 0.55 m		Field	Lab	Field	Lab	Bar crest	Bar fore slope	
Group 1 (G1)	L-N	Group 2 (G2)	H1–N	1.6	0.16	5.7	1.80	0	0	0
	L-CH		H1–CH	1.6	0.16	5.7	1.80	0.0314	0	0.0157
	L-CL		H1-CL	1.6	0.16	5.7	1.80	0.0157	0	0.0079
	L–CH–SH		H1-CH-SH	1.6	0.16	5.7	1.80	0.0314	0.0314	0.0232
	L-CL-SL		H1-CL-SL	1.6	0.16	5.7	1.80	0.0157	0.0157	0.0116
	L-CL-SH		H1-CL-SH	1.6	0.16	5.7	1.80	0.0157	0.0314	0.0154
	L–CH–SL		H1–CH-SL	1.6	0.16	5.7	1.80	0.0314	0.0157	0.0195
–		Group 3 (G3)	H2–N	2.1	0.21	6.7	2.12	0	0	0
–			H2–CH	2.1	0.21	6.7	2.12	0.0314	0	0.0157
–			H2-CL	2.1	0.21	6.7	2.12	0.0157	0	0.0079
–			H2-CH-SH	2.1	0.21	6.7	2.12	0.0314	0.0314	0.0232
–			H2-CL-SL	2.1	0.21	6.7	2.12	0.0157	0.0157	0.0116

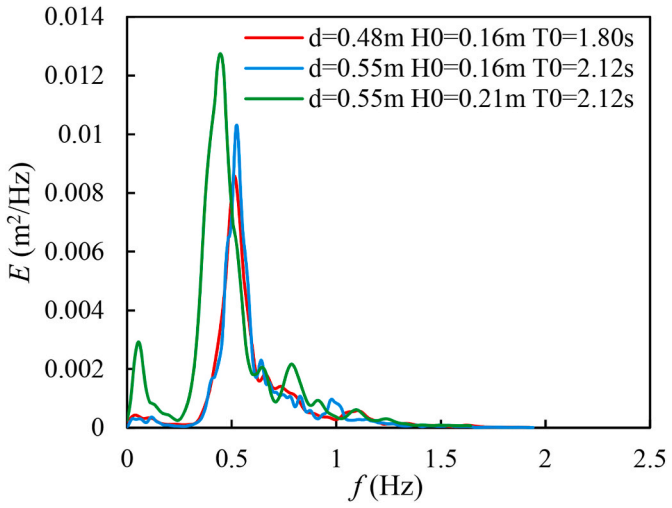

Fig. 5. Measured wave spectra in empty flume at gauge W0 for three incident wave conditions with still water depth (d) of 0.48 or 0.55 m.

and reflected wave amplitude a_r of each component, the wave reflection coefficient K_r can be obtained.

$$K_r = \left[\sum_{m=1}^{M} a_r^2(m) \Big/ \sum_{m=1}^{M} a_i^2(m) \right]^{1/2} \tag{3}$$

where M is a half of the total number of samples.

The incident wave height H_i and reflected wave height H_r can be calculated from K_r and the measured synthetic wave height H_s (the mean value of wave heights at W2 and W3) as follows.

$$\left.\begin{aligned} H_i &= H_s \Big/ \left(1 + K_r^2\right)^{1/2} \\ H_r &= K_r H_s \Big/ \left(1 + K_r^2\right)^{1/2} \end{aligned}\right\} \tag{4}$$

Transmitted wave height H_t was calculated from the wave data at W5, and the transmission coefficient K_t was given by $K_t = H_t/H_i$. Dissipation coefficient K_d represents wave energy loss, which can be calculated according to energy conservation (Yin et al., 2016; Ma et al., 2018a, 2018b), i.e.

$$K_r^2 + K_t^2 + K_d^2 = 1 \tag{5}$$

In order to quantify the vegetation influence on wave attenuation, the wave attenuation by vegetation was calculated by the following equation.

$$k_w = \frac{H_n - H_x}{H_n} \tag{6}$$

where H_x and H_n is the characteristic significant wave height at fore-dune (W7) in the test with and without vegetation.

Seabed profile change was obtained by image pixel analysis method. Firstly, the geomorphological contour image corresponding to the feature time in the video was intercepted and corrected, and then the geomorphological contour of the sandbar-lagoon system profile in each image was depicted with red single pixel points. The coordinates of red single pixel points were extracted with MATLAB through *RGB* color value, and finally the pixel coordinates were converted to the actual coordinate system shown in Fig. 1 to obtain the geomorphological profile change measurements.

3. Results

3.1. Wave transformation

The significant wave heights calculated from the wave spectrum measured by each wave gauge along the flume were plotted in Fig. 6. It can be seen that local wave height is increased with the decreased water depth over sandbar due to shoaling as shown in Li et al. (2021), and then wave height decreases rapidly after wave gauge Wa, and the significant wave height in lagoon with vegetation decreases more significantly compared with tests without vegetation. The greatest wave attenuation appears when high-density emergent vegetation was arranged on both the sea-side slope and the sandbar crest. When the wave propagates to the fore-dune, the wave height increases slightly due to the shallow water zone. When d = 0.55 m, it can be seen from Fig. 6b that vegetation significantly weakens the amplitude of increasing wave height in the margin of wave-breaking zone (Wa). The extreme point of increasing wave height moves towards the lagoon shown in Fig. 6c, from W4 (H2–N) without vegetation to Wa (H2–CH, H2-CL, vegetation only in sandbar crest) with vegetation. When d = 0.48 m, there is no obvious wave height change of different tests when the wave enters the shallow water area. It may be related to the zero freeboard (R_c, Bar crest elevation minus still water level) (Jones et al., 2013), which leads to not enough water depth for wave height change. Therefore, when R_c is the negative, emergent vegetation at the sandbar crest can weaken the amplitude of increasing wave height in the margin of wave-breaking zone, and when the incident wave height increases, the location of extreme wave height moves towards the lagoon.

Emergent vegetation reduces the wave height before and after vegetation canopy in general. But the wave height before vegetation

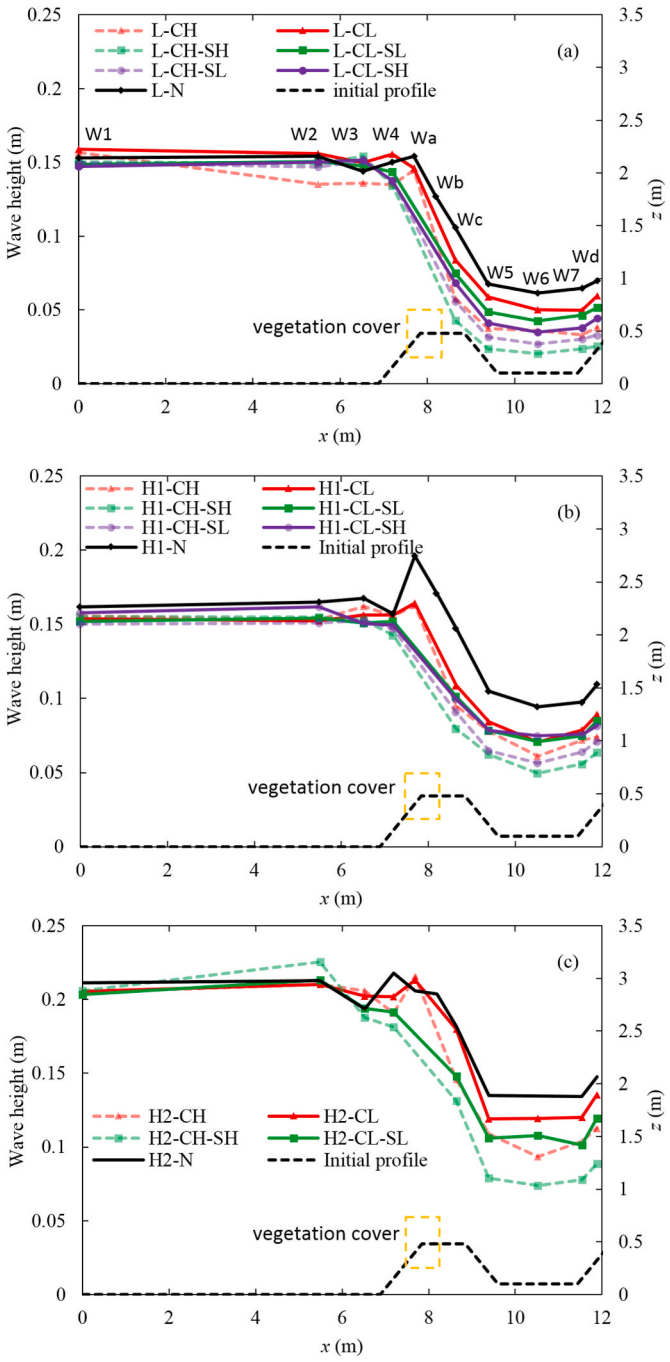

Fig. 6. Wave attenuation along the flume. (a) Group 1 (G1) with water depth d = 0.48 m and the incident significant wave height of 0.16 m; (b) Group 2 (G2) with d = 0.50 m and the incident wave height of 0.16 m; (c) Group 3 (G3) with d = 0.50 m and the incident wave height of 0.21 m. **L**: **L**ow water depth; **H1**: **H**igh water depth with H_0 of **0.16m**; **H2**: **H**igh water depth with H_0 of **0.21m**; **N**: **N**o vegetation; **CH**: Bar **C**rest with vegetation of **H**igh density; **SH**: Bar fore **S**lope with vegetation of **H**igh density; **CL**: Bar **C**rest with vegetation of **L**ow density; **SL**: Bar fore **S**lope with vegetation of **L**ow density.

cover is more complicated due to the presence of surf zone. For example, the attenuation characteristic at gauge W3 is almost completely different from that at gauge W4 in Group 3 (Fig. 6c). Besides, the position before vegetation was difficult to define due to different cover width of vegetation canopy. The magnitude of wave attenuation at W7 behind the vegetation cover is more obvious and Fig. 7 shows the corresponding wave attenuation coefficients. For same vegetation canopy, wave attenuation at gauge W7 for Group 1 (G1) is larger than that for Group 2

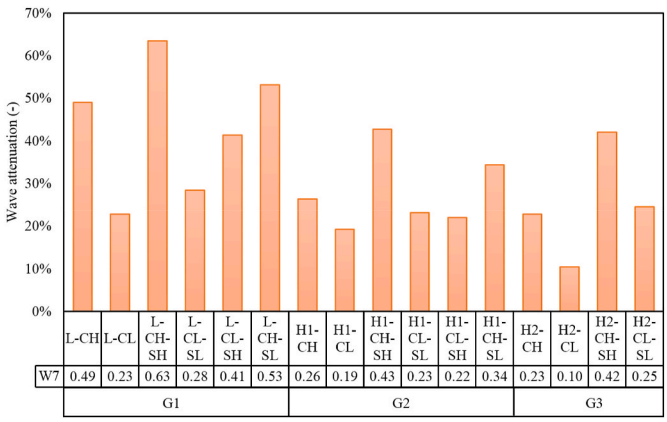

Fig. 7. Wave attenuation by vegetation canopy at Gauge W7. G1 is the Group with a freeboard R_c = 0, water depth d = 0.48 m and incident wave height of 0.16 m; G2 is the Group with R_c = −0.07 m, d = 0.55 m and incident wave height of 0.16 m; G3 is the Group with R_c = −0.07 m, d = 0.55 m and incident wave height of 0.21 m. **L**: **L**ow water depth; **H1**: **H**igh water depth with H_0 of **0.16m**; **H2**: **H**igh water depth with H_0 of **0.21m**; **N**: **N**o vegetation; **CH**: Bar **C**rest with vegetation of **H**igh density; **SH**: Bar fore **S**lope with vegetation of **H**igh density; **CL**: Bar **C**rest with vegetation of **L**ow density; **SL**: Bar fore **S**lope with vegetation of **L**ow density.

(G2) which is larger than that of Group 3 (G3), namely, when the freeboard R_c = 0 (G1, small water depth) the wave attenuation is the largest; as water depth increases (G2, G3; large water depth), the wave attenuation decreases. When the incident wave height increases (G3 from G2), the wave attenuation drops slightly. At Gauge W7, the maximum wave attenuation is 63.45% for G1, 42.74% for G2 and 42.02% for G3, respectively. Maximum wave attenuation is attained at the maximum weighted vegetation density for each group. In addition, for all tests, wave attenuation increases with increasing weighted vegetation density.

Fig. 8 illustrates the wave reflection, transmission, and dissipation coefficients. Overall, wave reflection coefficient K_r < wave transmission coefficient K_t < wave dissipation coefficient K_d, which is the same with Ma et al. (2018a) who studied on the effect of artificial reef. Given the same incident wave height, the K_r increases with decreasing freeboard so that K_r for group G1 (R_c = 0) is generally higher than that for G2 (R_c = −0.07 m). K_r increases (G2 < G3) with increasing incident wave height, affected by the freeboard R_c and the scarp shape of coastal fore-dune during erosion (further explained in the next subsection). When d = 0.48 m (G1), more waves break at the sandbar crest leading to a lower wave energy after the bar. Therefore, K_t of G1 is the lowest, due to its highest K_d. In addition, K_t in L–CH–SH and H2–N (abbreviations of different tests are shown in Table 1.) attains the minimum and maximum values, respectively. The smallest K_t may be due to lower energy after the sandbar caused by smaller water depth and the densest vegetation in L–CH–SH. However, the maximum K_t appears in H2–N, which may be caused by d = 0.55 m without vegetation.

3.2. Bed profile changes

Fig. 9 shows the geomorphological profiles after 2.73 min with sampling points of 8192 of each test. In general, the sea-side of sandbar crest is eroded more than the lagoon-side; the lagoon is almost always subject to deposition to various degrees. Scour hole is evident at the sea-side edge of vegetation canopy, where the sediment at the bed is stirred up and entrained by the enhanced local flow due to the oscillation of the vegetation mimics and blockage by vegetation canopy and wave reflection similar to the toe scour in front of a porous vertical breakwater and seawall studied by Peng et al. (2018) using a partial cell method. The result is consistent with the finding that roots may enhance erosion

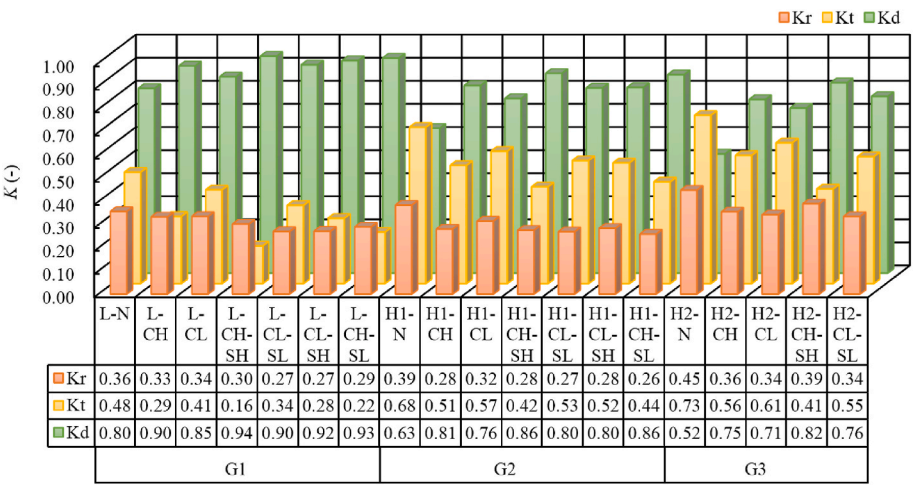

	L-N	L-CH	L-CL	L-CH-SH	L-CL-SL	L-CL-SH	L-CH-SL	H1-N	H1-CH	H1-CL	H1-CH-SH	H1-CL-SL	H1-CL-SH	H1-CH-SL	H2-N	H2-CH	H2-CL	H2-CH-SH	H2-CL-SL
Kr	0.36	0.33	0.34	0.30	0.27	0.27	0.29	0.39	0.28	0.32	0.28	0.27	0.28	0.26	0.45	0.36	0.34	0.39	0.34
Kt	0.48	0.29	0.41	0.16	0.34	0.28	0.22	0.68	0.51	0.57	0.42	0.53	0.52	0.44	0.73	0.56	0.61	0.41	0.55
Kd	0.80	0.90	0.85	0.94	0.90	0.92	0.93	0.63	0.81	0.76	0.86	0.80	0.80	0.86	0.52	0.75	0.71	0.82	0.76
	G1							G2							G3				

Fig. 8. Wave reflection, transmission, and dissipation coefficients. G1 is the group with a freeboard $R_c = 0$, water depth d = 0.48 m and incident wave height of 0.16 m; G2 is the group with $R_c = -0.07$ m, d = 0.55 m and incident wave height of 0.16 m; G3 is the group with $R_c = -0.07$ m, d = 0.55 m and incident wave height of 0.21 m. **L**: **L**ow water depth; **H1**: **H**igh water depth with H_0 of **0.16m**; **H2**: **H**igh water depth with H_0 of **0.21m**; **N**: **N**o vegetation; **CH**: Bar **C**rest with vegetation of **H**igh density; **SH**: Bar fore **S**lope with vegetation of **H**igh density; **CL**: Bar **C**rest with vegetation of **L**ow density; **SL**: Bar fore **S**lope with vegetation of **L**ow density.

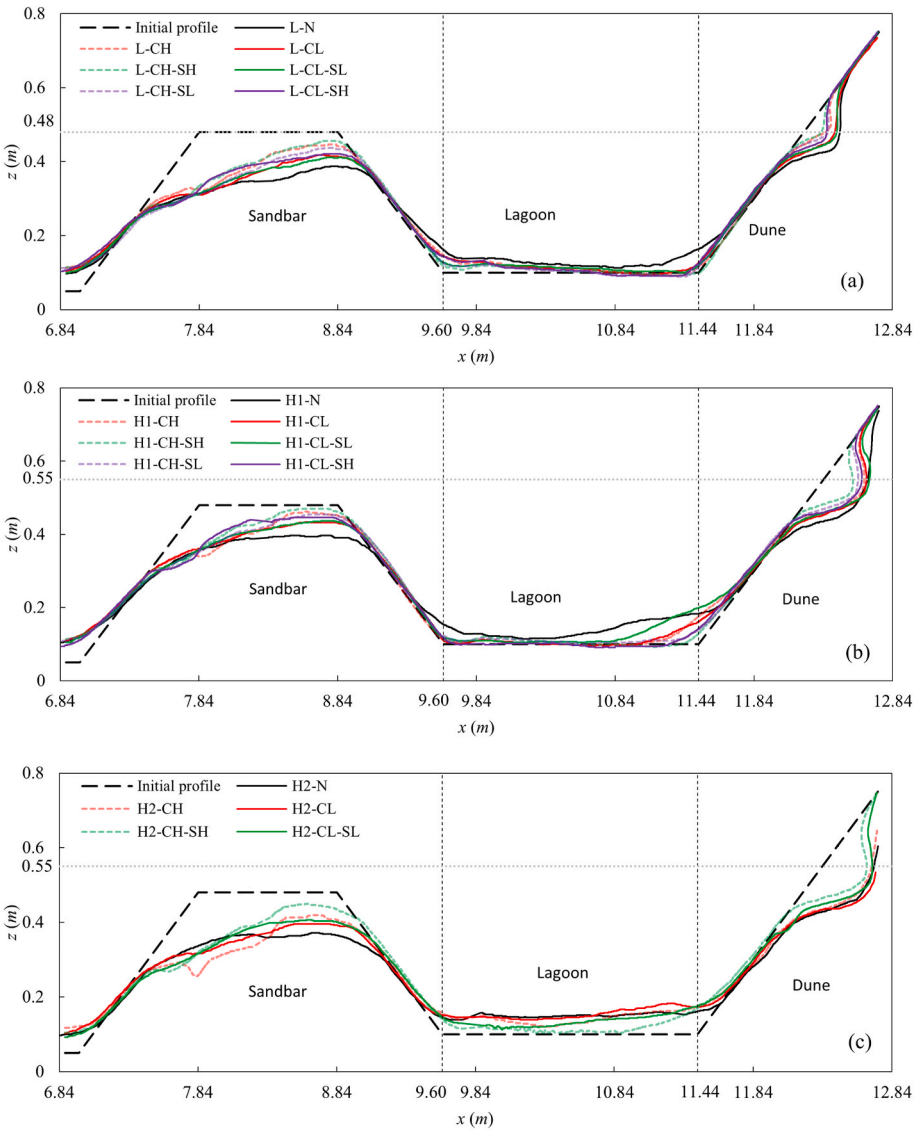

Fig. 9. Profile changes for: (a) G1, the Group 1 with a freeboard $R_c = 0$, water depth $d = 0.48$ m and incident wave height of 0.16 m; (b) G2, the Group 2 with $R_c = -0.07$ m, $d = 0.55$ m and incident wave height of 0.16 m; (c) G3, the Group3 with $R_c = -0.07$ m, $d = 0.55$ m and incident wave height of 0.21 m. The axes of x and z are the coordinate systems defined in Fig. 1. **L**: **L**ow water depth; **H1**: **H**igh water depth with H_0 of **0.16m**; **H2**: **H**igh water depth with H_0 of **0.21m**; **N**: **N**o vegetation; **CH**: Bar **C**rest with vegetation of **H**igh density; **SH**: Bar fore **S**lope with vegetation of **H**igh density; **CL**: Bar **C**rest with vegetation of **L**ow density; **SL**: Bar fore **S**lope with vegetation of **L**ow density.

through uprooting in marginal areas of salt marsh due to punctuated wave disturbances (Feagin et al., 2019) and that vegetation motion enhances turbulence energy, specifically at the interface of canopy and flow according to the coupled OpenFOAM-finite element model results by Chen and Zou (2019). Within the lagoon behind the sand bar, where water depth $d = 0.48$ m, more sediment accumulation occurs on the

bar-side for Group 1 (G1); however, when water depth $d = 0.55$ m, more sediment accumulation occurs on the dune-side for Group 2 and 3 (G2 and G3).

The collision regime is defined as the maximum run-up level remains under the elevation of dune crest, and the overwash regime was defined as the maximum run-up level exceeds the dune crest (Sallenger, 2000). The coastal fore-dune displays two kinds of scarp shape: s-shaped scarp (Fig. 10) and upward concave scarp (Fig. 11), corresponding to the collision and overwash regime, respectively, which is consistent with erosion regimes proposed by Silva et al. (2016) for the dune profiles with a berm. When $d = 0.48$ m (G1), the scarp becomes nearly vertical and tends to be s-shaped, which may cause waves to collide directly with the seaward face of the dune, resulting in strong wave reflection. When $d = 0.55$ m (G2), the scarp is s-shaped, and the convex shape above the scarp can buffer part of wave energy by changing wave shape to a roller and then a splashing (Fig. 10a and b) and reduce the wave reflection. Besides the cross-shore wave height transformation, skewness (*Sk*) and asymmetry (*As*) of wave profile relative to horizontal and vertical axes are the major drivers for wave-induced sediment transport and morphological change with and without low crest structure such as sand bar, reef and breakwater (Hoefel and Elgar, 2003; Ruessink et al., 2009; Gonzalez-Rodriguez and Madsen, 2007; Zou and Peng, 2011). Test video records indicate that overwash regime occurred in most tests of Group 3 (G3), i.e., when waves climb up the slope of fore-dune, cross the dune crest at 0.8 m elevation at $x = 12.84$ m and propagate down the lee slope of the dune (Fig. 11). In this regime, wave run-up promotes wave reflection as shown in Fig. 11c.

Interestingly, sand ripples occurred in the sandbar-side lagoon of H2-CH-SH and H2-CL-SL, which indicates stronger hydrodynamic effects near the lagoon bed. In order to assess whether ripples are present in other tests, recorded videos were watched carefully. Table 2 shows the presence and position of ripples in all the tests. When the water depth is 0.48 m and incident wave height is 0.16 m (group G1), ripples occur in L-N and L-CL when more wave energy propagates into lagoon. In group G2 (water depth of 0.55 m and incident wave height of 0.16 m), ripples occur in all tests except for H1-CH-SH when the highest vegetation density damps wave energy considerably. Thus it can be seen that the presence of ripples near the lagoon bed depends on the wave energy reached there. However, in group G3 which has higher incident wave height than group G2, ripples only occur in test runs of H2-CH-SH and H2-CL-SL when energy in lagoon is lower than other tests of G3. Further video observations indicate that a strong sediment transport prevents the formation of ripples. Because G1 has serious sedimentation near lagoon-side sandbar, ripples occur near the right side of lagoon. Ripples of G2 and G3 move to the left and/or middle of lagoon due to significant sediment transport in the dune-side lagoon. Therefore, the presence of ripples depend significantly on the wave energy dissipation and bed-load transport.

Maximum erosion and deposition thicknesses of sandbar ($x = 6.88$–9.60 m), lagoon ($x = 9.60$–11.44 m) and dune ($x = 11.44$–12.74 m) were derived from the measured bed profiles as shown in Fig. 12. The maximum erosion thickness is greater than the maximum deposition thickness. The maximum deposition thickness of sandbar remains between 5.2 cm and 7.4 cm for all three test groups of G1 to G3, and is mainly concentrated at the sea-side slope toe of the sandbar (Fig. 9). The maximum deposition thickness of lagoon and coastal fore-dune for G1 with a water depth $d = 0.48$ m is lower than that of G2 and G3 with a water depth $d = 0.55$ m. This is due to more wave breaking above the sandbar, which causes the lower wave energy being transmitted to the coastal fore-dune and less dune erosion at a shallower water depth $d = 0.48$ m of G1, as well as the maximum deposition thickness of lagoon near the sandbar-side and smaller deposition thickness at the fore-dune (Fig. 9a). However, when $d = 0.55$ m, the maximum deposition thicknesses of lagoon and fore-dune concentrated at the slope toe of the fore-dune becomes larger due to more dune erosion (Fig. 9b and c). In addition, the maximum deposition thicknesses of lagoon and dune for case H1-CL-SL is larger than that for other cases. It can be seen from Fig. 9b that the deposition slope of H1-CL-SL is significantly steeper than that of H1–N with more sediment transport towards lagoon near the dune toe, resulting in more deposition, so the maximum deposition thicknesses of lagoon and dune (H1-CL-SL) are larger.

With the same incident wave height, the maximum erosion thickness of sandbar for group G1 with a still water depth $d = 0.48$ m is slightly larger than that for group G2 with a water depth of $d = 0.55$ m due to

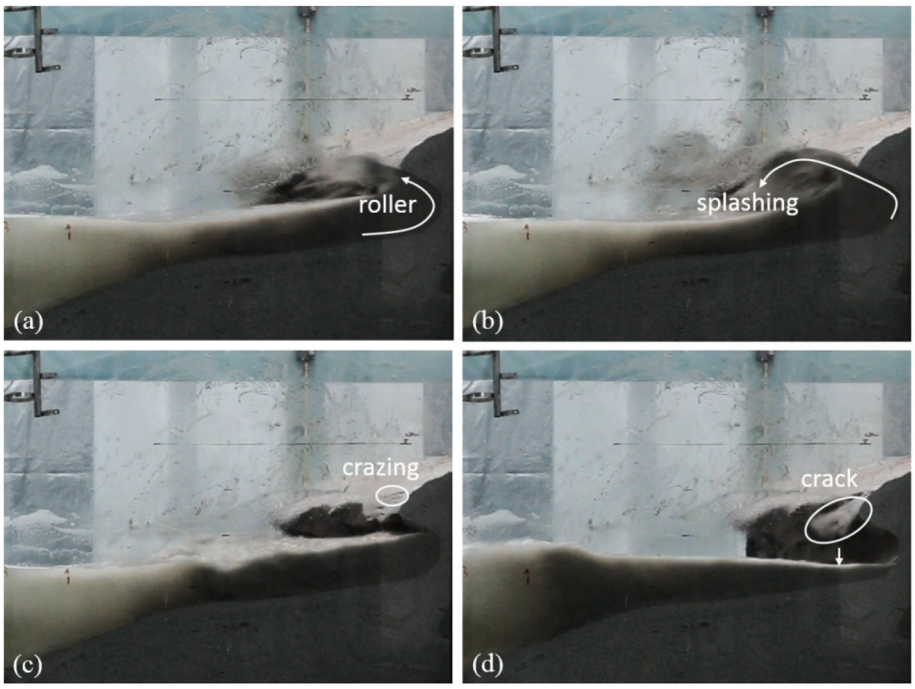

Fig. 10. Erosion process at the fore dune of s-shaped scarp (collision regime). (a) Roller generated by upward wave force; (b) Splashing formed with strong current against the dune barrier; (c) Crazing produced by continuing wave oscillation; and (d) Crack finally due to surpassed damage threshold.

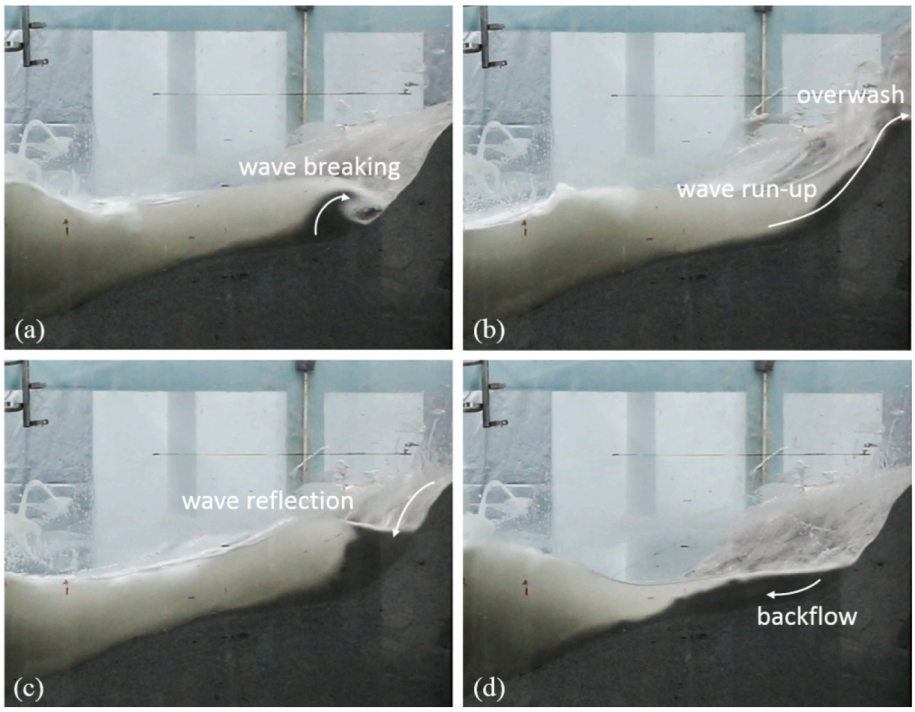

Fig. 11. Erosion process at the fore dune of upward concave scarp (overwash regime). (a) Wave breaking produced by shoaling effect; (b) Wave run-up leading to an overwash; (c) Wave reflection from fore-dune face; and (d) Backflow formed due to wave reflection.

Table 2
Presence and position of ripples in all tests derived from video observation. "√" represents a presence of ripples, while " × " represents an absence of ripples.

Test	Ripples	Position within lagoon	Test	Ripples	Position within lagoon	Test	Ripples	Position within lagoon
L-N	✓	Right	H1–N	✓	Left	H2–N	×	-
L-CH	×	-	H1–CH	✓	Left and middle	H2–CH	×	-
L-CL	✓	Right	H1-CL	✓	Left and middle	H2-CL	×	-
L–CH–SH	×	-	H1-CH-SH	×	-	H2-CH-SH	✓	Left and middle
L-CL-SL	×	-	H1-CL-SL	✓	Left and middle	H2-CL-SL	✓	Left
L-CL-SH	×	-	H1-CL-SH	✓	Left and middle	-	-	-
L–CH–SL	×	-	H1–CH-SL	✓	Left and middle	-	-	-

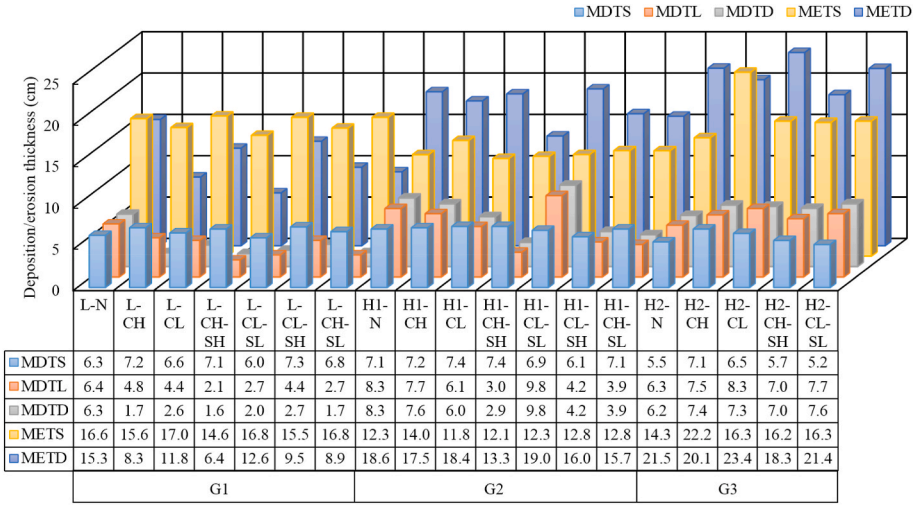

	L-N	L-CH	L-CL	L-CH-SH	L-CL-SL	L-CL-SH	L-CH-SL	H1-N	H1-CH	H1-CL	H1-CH-SH	H1-CL-SL	H1-CL-SH	H1-CH-SL	H2-N	H2-CH	H2-CL	H2-CH-SH	H2-CL-SL
MDTS	6.3	7.2	6.6	7.1	6.0	7.3	6.8	7.1	7.2	7.4	7.4	6.9	6.1	7.1	5.5	7.1	6.5	5.7	5.2
MDTL	6.4	4.8	4.4	2.1	2.7	4.4	2.7	8.3	7.7	6.1	3.0	9.8	4.2	3.9	6.3	7.5	8.3	7.0	7.7
MDTD	6.3	1.7	2.6	1.6	2.0	2.7	1.7	8.3	7.6	6.0	2.9	9.8	4.2	3.9	6.2	7.4	7.3	7.0	7.6
METS	16.6	15.6	17.0	14.6	16.8	15.5	16.8	12.3	14.0	11.8	12.1	12.3	12.8	12.8	14.3	22.2	16.3	16.2	16.3
METD	15.3	8.3	11.8	6.4	12.6	9.5	8.9	18.6	17.5	18.4	13.3	19.0	16.0	15.7	21.5	20.1	23.4	18.3	21.4
	G1							G2							G3				

Fig. 12. Maximum deposition and erosion thickness. MDTS: the maximum deposition thickness of sandbar; MDTL: the maximum deposition thickness of lagoon; MDTD: the maximum deposition thickness of dune; METS: the maximum erosion thickness of sandbar; METD: the maximum erosion thickness of dune. G1 is the group with a freeboard $R_c = 0$, water depth $d = 0.48$ m and incident wave height of 0.16 m; G2 is the group with $R_c = -0.07$ m, $d = 0.55$ m and incident wave height of 0.16 m; G3 is the group with $R_c = -0.07$ m, $d = 0.55$ m and incident wave height of 0.21 m.

more wave breaking and energy dissipation over the sandbar with a smaller water depth. The maximum erosion thickness of sandbar with emergent vegetation is larger than that without vegetation in some tests, especially in G3, which is consistent with the scour hole shown in Fig. 9c. The maximum erosion thickness of fore-dune with $d = 0.55$ m is larger (G2, G3) than that with $d = 0.48$ m (G1). Overall, the emergent aquatic vegetation reduces the maximum erosion thickness of fore-dune, but the test of H2-CL displays a larger maximum erosion thickness,

which may be due to the exposure of the rear PP board in the wave run-up process, hindering the overwash flow to a certain extent, and increasing the downward backflow and dune erosion.

4. Discussions

4.1. An empirical model of wave attenuation

In this study, the wave attenuation coefficient was calculated based on the wave height at the specific position of Gauge W7 of the test without vegetation, and more attention was paid to the vegetation effect. To quantitatively observe how the vegetation canopy affects wave attenuation, the best fitted line between wave attenuation and weighted vegetation density (ϕ_w) was shown in Fig. 13. Note that the condition without vegetation was taken as the origin of the axis (0, 0), and every intercept was artificially set as zero. Each group of data shows obvious linear correlation with all determination coefficients (R^2) greater than 0.93. In general, the weighted density of emergent vegetation considering the influence of cover width has a positive linear correlation with the wave attenuation coefficient in different groups.

Figs. 13a and b have a large difference in line slope, indicating that water depth d and freeboard R_c have a significant effect on wave attenuation. While, the similarity of line slope in Figs. 13b and c shows that the effect of incident wave height is slight. Due to a negative relationship between wave attenuation and d, a positive relationship between wave attenuation and R_c, and the same dimension of d, R_c, and weighted vegetation density, the following empirical formulas can be assumed.

$$k_w = a\frac{\phi_w}{d - iR_c} = a\zeta \ (a > 0) \tag{7}$$

where i is a factor representing the effect intensity of sandbar freeboard being changeable in the moveable bed of the sandbar-lagoon system; ζ is a new parameter containing vegetation density, water depth and sandbar freeboard, which is similar with Zhao et al. (2023). Fig. 14 presents a direct proportional relationship between wave attenuation and a new parameter. Note that the condition without vegetation was not considered in Fig. 14, but every intercept was artificially set as zero. We found that when $i = 3$ the determination coefficient R^2 reached the largest value of 0.95. It presents an optimally integrated relationship between wave damping and vegetation density. For sandbar-lagoon system, this relationship tells that weighted vegetation density, water depth and sandbar lagoon are the dominant factors, rather than incident wave height. The final formula $k_w = 13.31\zeta$ can be used to predict the wave attenuation in any typical lagoon-sandbar system affected by vegetation planted in sandbar, but more data is required for its calibration.

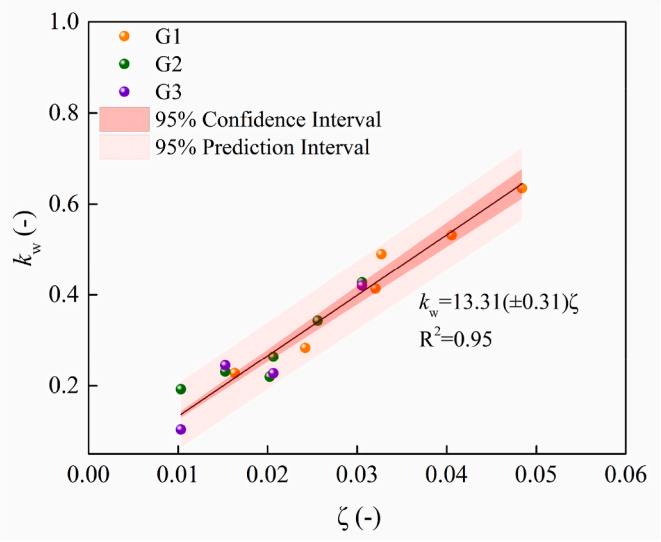

Fig. 14. Linear fitting of a new empirical formula of wave attenuation k_w with 95% confidence and prediction interval (band). Prediction band is to forecast variable, while confidence band is to forecast the desired value of variable. ζ is a new dimensionless parameter dependent on vegetation density, water depth and sandbar freeboard, similar with that in Zhao et al. (2023).

4.2. Relationship between wave coefficients and vegetation density

The relationship between weighted vegetation density and wave energy transformation described by wave reflection, transmission, and dissipation coefficient was demonstrated in. Fig. 15. The relationship between the reflection coefficient (K_r) and the weighted vegetation density (ϕ_w) is best fitted by a quadratic polynomial (Fig. 15a), especially at the water depth $d = 0.55$ m, with a determination coefficient greater than 0.94. At a water depth $d = 0.48$ m, the determination coefficient (ϕ_w and K_r) is lower, possibly due to complicated wave transformation. The wave reflection is initially and mainly influenced by the sandbar freeboard $R_c = 0$ and its steep seaward slope (Zhang et al., 2021a; Li et al., 2022b). As time goes by, the water depth over bar crest increases gradually, leading to strengthened effect of vegetation and fore-dune. With the increase of ϕ_w, K_r decreases first and then increases gradually. It is well known that when the water depth is smaller and the incident wave height is larger, ϕ_w corresponding to the minimum K_r is larger. Therefore, according to the fitting formula in the following chart, the order of ϕ_w corresponding to the minimum K_r are: G2 ($\phi_w = 0.0134$ m) <G1 ($\phi_w = 0.0172$ m) <G3 ($\phi_w = 0.0192$ m).

The wave transmission coefficient (K_t) decreases with increasing ϕ_w (Fig. 15b). The wave dissipation coefficient (K_d) increases with

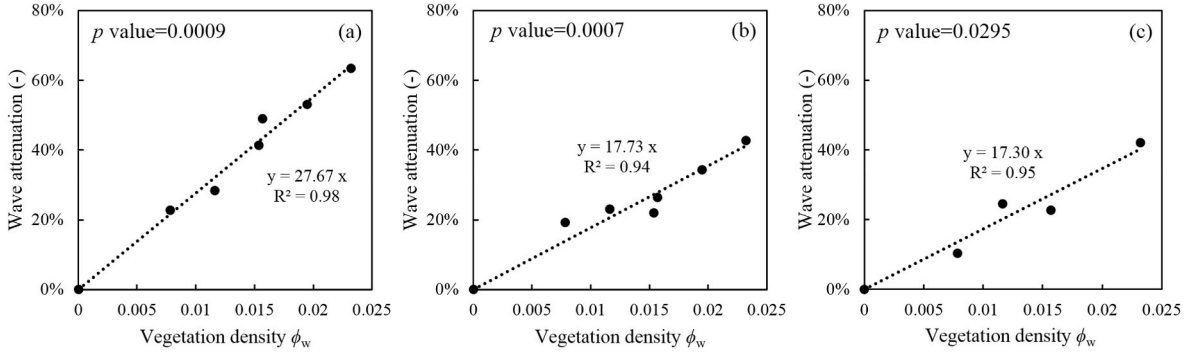

Fig. 13. Relationship between wave attenuation and weighted vegetation density. (a) Group G1, (b) Group G2 and (c) Group G3. G1 is the group with a freeboard $R_c = 0$, water depth $d = 0.48$ m and incident wave height of 0.16 m; G2 is the group with $R_c = -0.07$ m, $d = 0.55$ m and incident wave height of 0.16 m; G3 is the group with $R_c = -0.07$ m, $d = 0.55$ m and incident wave height of 0.21 m. p values were calculated using two-sided T-test with bi-sample equal variance hypothesis.

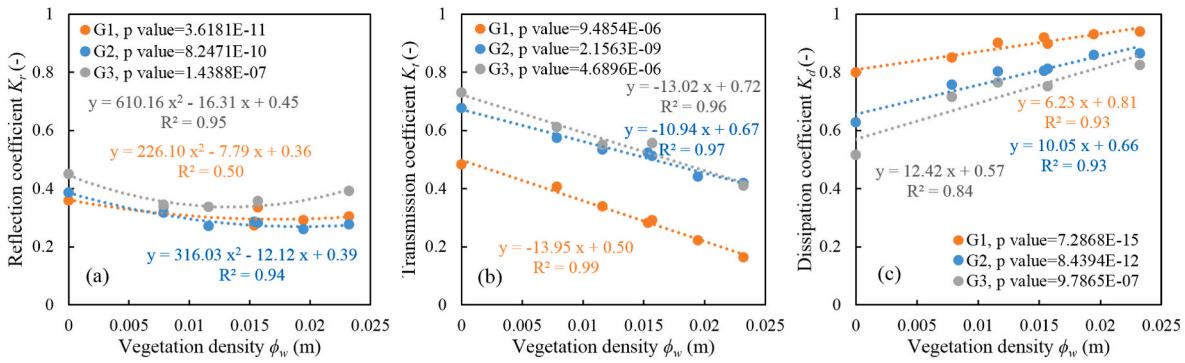

Fig. 15. Correlations between (a) wave reflection coefficient K_r, (b) wave transmission coefficient K_t, (c) wave dissipation coefficient K_d and weighted vegetation density ϕ_w. G1 is the group with a freeboard $R_c = 0$, water depth $d = 0.48$ m and incident wave height of 0.16 m; G2 is the group with $R_c = -0.07$ m, $d = 0.55$ m and incident wave height of 0.16 m; G3 is the group with $R_c = -0.07$ m, $d = 0.55$ m and incident wave height of 0.21 m.

increasing ϕ_w (Fig. 15c). The linear correlation between K_t or K_d and ϕ_w is excellent. Despite that the determination coefficient between K_d and ϕ_w of G3 is 0.84, the determination coefficient for other test groups (G1 and G3) is all greater than 0.92 with the highest value of 0.99. So, the following empirical formulas can be achieved.

$$\begin{cases} K_r = m_{r1}\phi_w^2 + m_{r2}\phi_w + m_{r0} & m_{r1} > 0, m_{r2} < 0 \\ K_t = m_{t1}\phi_w + m_{t0} & m_{t1} < 0, m_{t0} > 0 \\ K_d = m_{d1}\phi_w + m_{d0} & m_{d1} > 0, m_{d0} > 0 \end{cases} \tag{8}$$

where m_* (* represents different subscripts) are fitting coefficients. According to the quadratic polynomial correlation, there is an optimal vegetation density producing the least wave reflection coefficient. This would provide valuable guidance for engineering practice and a specific vegetation density range for lowest wave reflection. Wave transmission and dissipation are correlated to the wave attenuation (Fig. 13) linearly.

4.3. Dune protection by vegetation

Linear correlation between K_t or K_d and the maximum erosion thickness of fore-dune were proposed previously by Cong et al. (2021a). In that study, the incident wave height was 0.10 m, and the maximum erosion thickness of fore-dune was only 17 cm. While, in this study, intensive nonlinear relationship occurs due to larger wave energy, especially the group G3 with the maximum erosion thickness of fore-dune reaching to 23 cm. Dune erosion has been concerned carefully due to the decreasing coastal resilience. Fig. 16 presents a quadratic polynomial relationship between the weighted vegetation density (ϕ_w) and the maximum erosion thickness of fore-dune. When ϕ_w is small, the maximum erosion thickness of fore-dune changes slightly. In general, the maximum erosion thickness of fore-dune decreases almost linearly with increasing ϕ_w, especially G2 with determination coefficient in linear fit of 0.90 equivalent to that of quadratic polynomial fitting.

Overall, when the maximum erosion thickness of fore-dune is small, the relationship tends to be linear (Fig. 16a, G2); when the erosion is severe, the nonlinear interaction becomes prominent, showing an obvious quadratic polynomial correlation (Fig. 16a, G1 and G3). This relationship seems to correspond with wave reflection. The lowest reflection leads to the greatest erosion thickness. Taking the new parameter ζ ($i = 3$) mentioned above as the independent variable, and relative erosion thickness E_d/H_0 as the dependent variable, the following empirical formulas are derived.

$$\frac{E_d}{H_0} = b_2\zeta^2 + b_1\zeta + b_0 \tag{9}$$

where E_d is the maximum erosion thickness of dune; b_* (* represents different subscripts) are the fitting coefficients. The quadratic polynomial relationship in Fig. 16a indicates that too sparse vegetation cover may lead to more erosion for nature-based engineering design. Fig. 16b demonstrates that water depth and sandbar freeboard are important design considerations. This provides a scientific guide for ecological restoration projects. Meanwhile, this helps to explain the worst ecological degradation. When the vegetation cover area is reduced to a critical value, the erosion will be intensified and then the ecological environment degrades. These results also show that it is critical to conduct anthropogenic ecological restoration projects for eroded coasts.

This study improves our understanding of the mechanism for the vegetation to influence the sandbar-lagoon systems and provides the

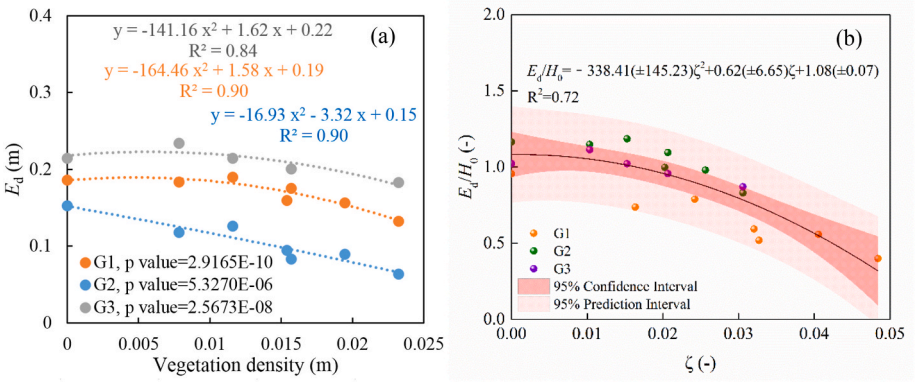

Fig. 16. Correlations between the weighted vegetation density ϕ_w and the maximum erosion thickness of dune (a); relationship between ζ and relative erosion thickness E_d/H_0 (b). G1 is the group with a freeboard $R_c = 0$, water depth $d = 0.48$ m and incident wave height of 0.16 m; G2 is the group with $R_c = -0.07$ m, $d = 0.55$ m and incident wave height of 0.16 m; G3 is the group with $R_c = -0.07$ m, $d = 0.55$ m and incident wave height of 0.21 m.

design guidance for nature-based coastal defense projects. The vegetation roots were not considered in this study since the uprooting did not occur, however, the enhanced erosion due to the oscillation of mimics is consistent with previous finding (Feagin et al., 2019) that more erosion at the sea-side margin of vegetation cover during high sea states. In addition, the influence of the annual growth cycle of vegetation (Paul and Kerpen, 2021) on the flora and fauna in sandbar-lagoon system is not well understood and not included in this study. On the other hand, short-term sediment disturbance regimes (Cao et al., 2018), shoot stiffness (Bouma et al., 2009) and wave attack (Silinski et al., 2018; Cao et al., 2020) have significant effects on seedling establishment. So interdisciplinary collaboration among geomorphologists, plant and environmental researchers is required to improve our understanding of the vegetated coastal system.

5. Conclusion

An experimental study of a sandbar-lagoon system was conducted to investigate how vegetation canopy influences wave propagation and transformation and the response of morphodynamic evolution to wave attack. A sandbar-lagoon bed profile, without and with vegetation canopy of different densities in sandbar, was investigated by nineteen tests of three groups in a wave flume. Experimental results indicated that the weighted vegetation density considering the distribution width in the direction of wave propagation has different relationship with the wave attenuation coefficient and the maximum erosion thickness of dune.

A weighted density by the width of vegetation cover was presented and an empirical linear relationship between wave attenuation and a new parameter dependent on water depth and sandbar freeboard for the sandbar-lagoon system was provided. It was found that the wave attenuation increases with the rise of sandbar freeboard and the weighted vegetation density, and decreases with the fall of incident wave height. In addition, the wave reflection coefficient has a quadratic polynomial relationship with the vegetation density. The wave transmission and dissipation coefficients have a negative and a positive linear relationship with vegetation density, respectively. There is an optimal vegetation density for the least wave reflection due to the quadratic polynomial correlation.

The sea-side of sandbar crest is eroded more than the lagoon-side. The lagoon is almost always where the sand accumulates. The coastal fore-dune exhibits s-shaped scarp for the collision regime and upward concave scarp for the overwash regime. When overwash occurs more frequently than collision, it is easier to form a vertical shape of scarp due to wave run-up, which increases the wave reflection to some extent. The maximum erosion thickness is greater than the maximum deposition thickness, which indicates that the extent of deposition is larger in order to satisfy the mass conservation of sediment. The maximum erosion thickness of dune follows a quadratic polynomial relationship with vegetation density; therefore, too sparse vegetation cover may lead to more erosion. However, when the maximum erosion thickness of fore-dune is smaller, this relationship becomes linear. In general, water depth, wave height and sandbar freeboard are also important contributing factors to wave attenuation, apart from vegetation density. These relationships provide a scientific guide for green coastal defense and coastal ecological restoration projects, especially in the sandbar-lagoon system.

Author credit statement

Xin Cong: Experiments, Data analysis, Writing–original draft. Cuiping Kuang: Conceptualization, Methodology, Writing–review & editing, Supervision, Funding acquisition. Guangwei Huang: Experiments. Qingping Zou: Discussion, Writing–review & editing. Xuejian Han: Experiment guidance. Chao Shen: Instruments operation teaching in experiments. Jie Gu: Discussion.

Declaration of competing interest

The authors declare that they have no known competing financial interests or personal relationships that could have appeared to influence the work reported in this paper.

Data availability

Data will be made available on request.

Acknowledgements

This study was supported by the National Natural Science Foundation of China (Grant No. 41976159) and the National Key Research and Development Program of China (Grant No. 2022YFC3106205). Professor Qingping Zou has been supported by the Natural Environment Research Council of UK (Grant No. NE/V006088/1).

Appendix. Physical model scaling

Light-weight resin sand with a median particle size of 0.15–0.18 mm and density of 1.40–1.45 g/cm^3 were selected so that the average particle size of 0.17 mm and density of 1.43 g/cm^3 were used in the following scaling analysis. According to the field measurements near Qilihai lagoon, the average particle size was 0.12 mm at the study area. The area within 1 km seaward from the tidal inlet with a particle size from 0.08 mm to 0.32 mm was simulated by the present flume experiment.

Shields and Rouse scaling were adopted to ensure the sediment transport similitude between the prototype and the physical model, Froude number similitude is used to down scaling the prototype hydrodynamics to the physical model hydrodynamics. Froude number F (A1), critical Shields number ψ_c (A2), critical bed shear stress τ_c (A3), wave friction coefficient f_w (A4), relationship between ψ_c and dimensionless grain size D_* (A5), Rouse number Rou (A8) and settling velocity ω_s (A9) are used in the scaling. The Froude number is given by

$$F = \frac{\pi H_s}{T\sqrt{gh}} \tag{A1}$$

where H_s is the significant wave height; T is the wave period; h is the water depth; g is the gravitational acceleration, which is 9.81 m/s^2. The critical Shields number is given by

$$\psi_c = \frac{\tau_c}{(\rho_s - \rho)gD} \tag{A2}$$

Where ρ is the water density; ρ_s is the sediment grain density; D is the sediment grain size; the critical bed shear stress τ_c is dominated by the wave contribution (Zou 2004), i.e.,

$$\tau_c = \tau_w = \frac{1}{2}\rho f_w U_w^2 \tag{A3}$$

where U_w is the wave orbital velocity amplitude at sea bed; f_w is the bed friction factor. In this study, the vegetation zone with lower water depth where the profile change depends largely on wave breaking, therefore, the rough-bed wave friction factor was adopted (Zou and Hay 2003),

$$f_w = 0.237\left(\frac{A}{k_s}\right)^{-0.52} \tag{A4}$$

where $A = \frac{U_w T}{2\pi}$ is the orbital amplitude of wave motion at the bed; k_s is the Nikuradse equivalent sand grain roughness which is 2.5 times the grain diameter. The critical shields number ψ_c is related to the dimensionless grain size D_* by

$$\begin{aligned} D_* &= D\left[(s-1)\frac{g}{\nu^2}\right]^{1/3} \\ \psi_c &= \frac{0.30}{1+1.2D_*} + 0.055[1-\exp(-0.02D_*)] \end{aligned} \tag{A5}$$

where $s = \rho_s/\rho$ is the ratio of density of grain and water which is between 2.0–8.0 according to the prototypical sediment grain size of 0.08–0.32 mm. For this grain size range, the relationship (A5) was re-fitted linearly over a logarithmic scale with a determination coefficient of 0.998. Accordingly, Equation (A5) reduces to

$$\psi_c = 0.14 D_*^{-0.66} \tag{A6}$$

Combining Equations (A1) to (A6), scale factor is obtained

$$\lambda_l = \lambda_{s-1}^{1.62}\lambda_D^{-0.38} \tag{A7}$$

where the scaling factor λ related the variable in prototype to its physical model value; $\lambda_{s\text{-}1}$, λ_D and λ_l is the scaling factor of sediment incipient motion relating the scales of submerged relative density s - 1, sediment grain size D and length l, respectively. According to the chosen model sand of light-weight resin sand, different prototype grain size could be obtained. Considering the flume size and incident wave condition, we chose the length scale of $\lambda_l = 10$. Accordingly, the model sand grain size of 0.17 mm is corresponding to the prototype size of 0.12 mm, which is in the range of 0.08–0.32 mm. The Rouse number represents the ratio between settling velocity and turbulent velocity i.e.,

$$Rou = \frac{\omega_s}{u'} \tag{A8}$$

where $u' = 2\pi\kappa\sqrt{f_w/2}A/T$ is the turbulence velocity; $\kappa = 0.40$ is the von Karman's constant; the sediment settling velocity $\omega_s \approx 0.0057 - 0.047$ m/s of model sand was given by

$$\omega_s = \frac{(s-1)gD^2}{18\nu}, \quad 0.001\text{mm} < D \le 0.1\text{mm} \tag{A9a}$$

$$\omega_s = \frac{10\nu}{D}\left[\left(1+\frac{0.01(s-1)gD^3}{\nu^2}\right)^{0.5} - 1\right], \quad 0.1\text{mm} < D < 1\text{mm} \tag{A9b}$$

For the grain size of model sand of 0.17 mm, the settling velocity of 0.0058 m/s can be obtained from (A9). Rouse number varies with wave parameters as well. According to Equation (A1), (A4) and (A8), the scaling factor of settling velocity ω, grain size D and length l was related to each other by the combining scales of sediment settling similitude and hydrodynamic similitude as

$$\lambda_\omega = \lambda_l^{0.24}\lambda_D^{0.26} \tag{A10}$$

For a length scale of 10, the model sand grain size of 0.17 mm, and settling velocity of 0.0058 m/s, the prototype sand grain sizes of 0.10 mm (A9a) and 0.11 mm (A9b) were determined and they were all in prototypical sand size range. In summary, the length scale of 10 was selected for the present study, with the wave height scale of 10 and wave period scale of $\sqrt{10}$.

References

Anderson, M.E., Smith, J.M., 2014. Wave attenuation by flexible, idealized salt marsh vegetation. Coast. Eng. 83, 82–92.

Augustin, L.N., Irish, J.L., Lynett, P., 2009. Laboratory and numerical studies of wave damping by emergent and near-emergent wetland vegetation. Coast. Eng. 56 (3), 332–340.

Astudillo, C., Gracia, V., Cáceres, I., Sierra, J.P., Sánchez-Arcilla, A., 2022. Beach profile changes induced by surrogate Posidonia oceanica: laboratory experiments. Coast. Eng. 175, 104144.

Ayat, B., Kobayashi, N., 2015. Vertical cylinder density and toppling effects on dune erosion and overwash. J. Waterw. Port, Coast. Ocean Eng. 141 (1), 04014026.

Bouma, T.J., Friedrichs, M., Klaassen, P., Van Wesenbeeck, B.K., Brun, F.G., Temmerman, S., van Katwijk, M.M., Graf, G., Herman, P.M.J., 2009. Effects of shoot stiffness, shoot size and current velocity on scouring sediment from around seedlings and propagules. Mar. Ecol.: Prog. Ser. 388, 293–297.

Cao, H.B., Zhu, Z.C., Balke, T., Zhang, L., Bouma, T.J., 2018. Effects of sediment disturbance regimes on Spartina seedling establishment: implications for salt marsh creation and restoration. Limnol. Oceanogr. 63 (2), 647–659.

Cao, H.B., Zhu, Z.C., James, R., Herman, P.M., Zhang, L.Q., Yuan, L., Bouma, T.J., 2020. Wave effects on seedling establishment of three pioneer marsh species: survival, morphology and biomechanics. Ann. Bot. 125 (2), 345–352.

Chen, H., Zou, Q.P., 2019. Eulerian-Lagrangian flow-vegetation interaction model using immersed boundary method and OpenFOAM. Adv. Water Resour. 126, 176–192.

Chen, Q., Zhao, H.H., 2012. Theoretical models for wave energy dissipation caused by vegetation. J. Eng. Mech. 138 (2), 221–229.

Clara, I., Dyack, B., Rolfe, J., Newton, A., Borg, D., Povilanskas, R., Brito, A.C., 2017. The value of coastal lagoons: case study of recreation at the Ria de Aveiro, Portugal in comparison to the Coorong, Australia. J. Nat. Conserv. 43, 190–200.

Cong, X., Kuang, C.P., Liu, H.X., Zhu, L., Shen, C., 2022. Experimental observation on wave and profile changes in a sandbar-lagoon system by submerged vegetation on the sandbar slope. In: Proceedings of Coasts and Ports 2021 Conference, pp. 1014–1019.
Cong, X., Kuang, C.P., Han, X.J., Gong, L.X., Shen, C., 2021a. Experimental observation on wave and profile changes in a sandbar-lagoon system with emergent aquatic plants on the sandbar crest. In: The 31st International Ocean and Polar Engineering Conference, pp. 2216–2222.
Cong, X., Kuang, C.P., Wu, Y.L., Xia, Z.L., 2021b. Study on erosion and deposition in a sandbar-lagoon system influenced by submerged vegetation under erosion wave conditions. J. Trop. Oceanogr. 41 (4), 31–37.
Costanza, R., d'Arge, R., De Groot, R., Farber, S., Grasso, M., Hannon, B., Limburg, K., Naeem, S., O'neill, R.V., Paruelo, J., Raskin, R.G., 1997. The value of the world's ecosystem services and natural capital. Nature 387, 253–260.
Dalrymple, R.A., Kirby, J.T., Hwang, P.A., 1984. Wave diffraction due to areas of energy dissipation. J. Waterw. Port, Coast. Ocean Eng. 110 (1), 67–79.
Feagin, R.A., Furman, M., Salgado, K., Martínez, M.L., Innocenti, R.A., Eubanks, K., Figlus, J., Huff, T.P., Sigren, J., Silva, R., 2019. The role of beach and sand dune vegetation in mediating wave run up erosion. Estuarine Coast Shelf Sci. 219, 97–106.
Figlus, J., Sigren, J.M., Power, M.J., Armitage, R.A., 2017. Physical model experiment investigating interactions between different dune vegetation and morphology changes under wave impact. In: Proceedings of Coastal Dynamics, pp. 470–480.
Fu, G.Q., Xu, X.Y., Qiu, X.N., Xu, G.X., Shang, W., Yang, X.M., Zhao, P., Chai, C., Hu, X. K., Zhang, Y., Wang, Q.Q., Zhao, C.Y., 2021. Wind tunnel study of the effect of planting Haloxylon ammodendron on aeolian sediment transport. Biosyst. Eng. 208, 234–245.
Goda, Y., Suzuki, 1976. Estimation of incident and reflected waves in random wave experiments. In: Proceedings of the 15th International Conference on Coastal Engineering, vol. 15. ICCE, Hawaii, pp. 828–845.
Gonzalez-Rodriguez, D., Madsen, O.S., 2007. Seabed shear stress and bedload transport due to asymmetric and skewed waves. Coast. Eng. 54 (12), 914–929.
Han, X.J., Kuang, C.P., Zhu, L., Gong, L.X., Cong, X., 2022. Hydrodynamical and morphological patterns of a sandy coast with a beach nourishment suffering from a storm surge. Coast Eng. J. 64 (1), 83–99.
Hanley, M.E., Bouma, T.J., Mossman, H.L., 2020. The gathering storm: optimizing management of coastal ecosystems in the face of a climate-driven threat. Ann. Bot. 125 (2), 197–212.
Higuera, P., Lara, J.L., Losada, I.J., 2013. Realistic wave generation and active wave absorption for Navier-Stokes models. Coast. Eng. 71, 102–118.
Hoefel, F., Elgar, S., 2003. Wave-induced sediment transport and sandbar migration. Science 299 (5614), 1885–1887.
Jackson, D., Short, A., 2020. Sandy Beach Morphodynamics. Elsevier.
Jacobsen, N., McFall, B., van der A, D., 2019. A frequency distributed dissipation model for canopies. Coast. Eng. 150, 135–146.
Jones, D.K., Zou, Q.P., Reeve, D.E., 2013. Computational modelling of coastal flooding caused by combined surge overflow and wave overtopping on embankments. J. Flood Risk Manag. 6 (2), 70–84.
Kirwan, M.L., Megonigal, J.P., 2013. Tidal wetland stability in the face of human impacts and sea-level rise. Nature 504 (7478), 53–60.
Kobayashi, N., Raichle, A.W., Asano, T., 1993. Wave attenuation by vegetation. J. Waterw. Port, Coast. Ocean Eng. 119 (1), 30–48.
Koftis, T., Prinos, P., Stratigaki, V., 2013. Wave damping over artificial Posidonia oceanica meadow: a large-scale experimental study. Coast. Eng. 73, 71–83.
Kuang, C.P., Huang, G.W., Cong, X., Liu, H.X., Zhu, L., 2021. Experimental study on wave attenuation by a sandbar with emerged rigid vegetation. In: The 31st International Ocean and Polar Engineering Conference, pp. 2211–2215.
Kuang, C.P., Ma, Y., Han, X.J., Pan, S.Q., Zhu, L., 2020. Experimental observation on beach evolution process with presence of artificial submerged sand bar and reef. J. Mar. Sci. Eng. 8 (12), 1019.
Lei, J., Nepf, H., 2019. Wave damping by flexible vegetation: connecting individual blade dynamics to the meadow scale. Coast. Eng. 147, 138–148.
Li, H.R., Liu, C.C., Cheng, H., Zou, X.Y., Zhang, C.L., Liu, B., Li, J.F., Kang, L.Q., Wu, Y.Q., 2022a. A general model for predicting aeolian transport rate over sand surfaces with vegetation cover. Earth Surf. Processes Landforms 47 (10), 2471–2482.
Li, Y., Zhang, C., Cai, Y., Xie, M.X., Qi, H.S., Wang, Y.G., 2021. Wave dissipation and sediment transport patterns during shoreface nourishment towards equilibrium. J. Mar. Sci. Eng. 9 (5), 535.
Li, Y., Zhang, C., Dai, W.Q., Chen, D.K., Sui, T.T., Xie, M.X., Chen, S.G., 2022b. Laboratory investigation on morphology response of submerged artificial sandbar and its impact on beach evolution under storm wave condition. Mar. Geol. 443, 106668.
Lowe, R.J., Koseff, J.R., Monismith, S.G., 2005. Oscillatory flow through submerged canopies: 1. Velocity structure. J. Geophys. Res.: Oceans 110 (C10).
Luhar, M., Infantes, E., Nepf, H., 2017. Seagrass blade motion under waves and its impact on wave decay. J. Geophys. Res.: Oceans 122 (5), 3736–3752.
Ma, Y., Kuang, C.P., Han, X.J., Niu, H.B., Zheng, Y.H., Shen, C., 2020. Experimental study on the influence of an artificial reef on cross-shore morphodynamic processes of a wave-dominated beach. Water 12 (10), 2497.
Ma, Y., Kuang, C.P., Han, X.J., Dong, B.L., 2018a. Wave attenuation mechanism of the artificial reef in Beidaihe, China. In: The 28th International Ocean and Polar Engineering Conference. OnePetro, pp. 1446–1452.
Ma, Y., Kuang, C.P., Han, X.J., Zhu, L., 2018b. Experimental investigation on regular wave process through an artificial reef. In: The Thirteenth ISOPE Pacific/Asia Offshore Mechanics Symposium. OnePetro, pp. 96–104.
Manca, E., Cáceres, I.J.V.I., Alsina, J.M., Stratigaki, V., Townend, I., Amos, C.L., 2012. Wave energy and wave-induced flow reduction by full-scale model Posidonia oceanica seagrass. Continent. Shelf Res. 50, 100–116.
Maza, M., Lara, J.L., Losada, I.J., 2022. A paradigm shift in the quantification of wave energy attenuation due to saltmarshes based on their standing biomass. Sci. Rep. 12 (1), 13883.
Maza, M., Lara, J.L., Losada, I.J., Ondiviela, B., Trinogga, J., Bouma, T.J., 2015. Large-scale 3-D experiments of wave and current interaction with real vegetation. Part 2: experimental analysis. Coast. Eng. 106, 73–86.
Mendez, F.J., Losada, I.J., 2004. An empirical model to estimate the propagation of random breaking and nonbreaking waves over vegetation fields. Coast. Eng. 51, 103–118.
Möller, I., Kudella, M., Rupprecht, F., Spencer, T., Paul, M., Van Wesenbeeck, B.K., Wolters, G., Jensen, K., Bouma, T.J., Miranda-Lange, M., Schimmels, S., 2014. Wave attenuation over coastal salt marshes under storm surge conditions. Nat. Geosci. 7 (10), 727–731.
Möller, I., Mantilla-Contreras, J., Spencer, T., Hayes, A., 2011. Micro-tidal coastal reed beds: hydro-morphological insights and observations on wave transformation from the southern Baltic Sea. Estuarine Coastal Shelf Sci. 92 (3), 424–436.
Morris, R.L., Konlechner, T.M., Ghisalberti, M., Swearer, S.E., 2018. From grey to green: efficacy of eco-engineering solutions for nature-based coastal defense. Global Change Biol. 24, 1827–1842.
Odériz, I., Knöchelmann, N., Silva, R., Feagin, R.A., Martínez, M.L., Mendoza, E., 2020. Reinforcement of vegetated and unvegetated dunes by a rocky core: a viable alternative for dissipating waves and providing protection? Coast. Eng. 158, 103675.
Ozeren, Y., Wren, D.G., Wu, W., 2014. Experimental investigation of wave attenuation through model and live vegetation. J. Waterw. Port, Coast. Ocean Eng. 140 (5), 04014019.
Pan, Y., Chen, Y.P., Zhang, T.X., Hu, Y.Z., Yin, S., Yang, Y.B., Tan, H.M., 2018. Laboratory study on erosion of vegetated HPTRM system under high-speed open-channel flow. J. Waterw. Port, Coast. Ocean Eng. 144 (1), 04017038.
Pan, Y., Qu, X.K., Yang, Y.B., Zhang, J.B., Wang, G., Yin, S., Chen, Y.P., 2023. Laboratory experiments on the evolution of a submerged berm driven by low-energy irregular waves. Coast. Eng. 182, 104301.
Pan, Y., Yin, S., Chen, Y.P., Yang, Y.B., Xu, C.Y., Xu, Z.S., 2022. An experimental study on the evolution of a submerged berm under the effects of regular waves in low-energy conditions. Coast. Eng. 176, 104169.
Paul, M., Bouma, T.J., Amos, C.L., 2012. Wave attenuation by submerged vegetation: combining the effect of organism traits and tidal current. Mar. Ecol.: Prog. Ser. 444, 31–41.
Paul, M., Kerpen, N.B., 2021. Erosion protection by winter state of salt marsh vegetation. J. Ecohydraul. 7 (2), 144–153.
Peng, Z., Zou, Q.P., Lin, P.Z., 2018. A partial cell technique for modeling the morphological change and scour. Coast. Eng. 131, 88–105.
Ponsioen, L., van Damme, M., Hofland, B., Peeters, P., 2019. Relating grass failure on the landside slope to wave overtopping induced excess normal stresses. Coast. Eng. 148, 49–56.
Rupprecht, F., MÖLler, I., Paul, M., Kudella, M., Spencer, T., van Wesenbeeck, B.K., Wolters, G., Jensen, K., Bouma, T.J., Miranda-Lange, M., Schimmels, S., 2017. Vegetation-wave interactions in salt marshes under storm surge conditions. Ecol. Eng. 100, 301–315.
Ruessink, B.G., van den Berg, T.J.J., van Rijn, L.C., 2009. Modeling sediment transport beneath skewed asymmetric waves above a plane bed. J. Geophys. Res. Oceans 114, C11021.
Sallenger, A.H., 2000. Coastal of Florida summer storm impact scale for barrier islands. J. Coast Res. 16 (3), 890–895.
Silinski, A., Schoutens, K., Puijalon, S., Schoelynck, J., Luyckx, D., Troch, P., Meire, P., Temmerman, S., 2018. Coping with waves: plasticity in tidal marsh plants as self-adapting coastal ecosystem engineers. Limnol. Oceanogr. 63 (2), 799–815.
Silva, R., Martínez, M.L., Odériz, I., Mendoza, E., Feagin, R.A., 2016. Response of vegetated dune–beach systems to storm conditions. Coast. Eng. 109, 53–62.
Stratigaki, V., Manca, E., Prinos, P., Losada, I.J., Lara, J.L., Sclavo, M., Amos, C.L., Cáceres, I., Sánchez-Arcilla, A., 2011. Large-scale experiments on wave propagation over Posidonia oceanica. J. Hydraul. Res. 49, 31–43.
Suresh, K., Khanal, U., Wilson, C., 2021. Stakeholders' use and preservation valuation of lagoon ecosystems. Econ. Anal. Pol. 71, 123–137.
Tanino, Y., Nepf, H.M., 2008. Laboratory investigation of mean drag in a random array of rigid, emergent cylinders. J. Hydraul. Eng. 134 (1), 34–41.
Türker, U., Kabdasli, M.S., 2004. Average sediment dislocation analysis for barred profiles. Ocean Eng. 31 (14/15), 1741–1756.
Türker, U., Yagci, O., Kabdasli, M.S., 2019. Impact of nearshore vegetation on coastal dune erosion: assessment through laboratory experiments. Environ. Earth Sci. 78 (19), 584.
Wu, W.C., Cox, D.T., 2015. Effects of wave steepness and relative water depth on wave attenuation by emergent vegetation. Estuar. Coast Shelf Sci. 164, 443–450.
Yin, S., Pan, Y., Chen, Y.P., 2017. Scale design based on local curve fitting method for low-energy sandy beach. Hydro-Sci. Eng. 4, 43–51.
Yin, Z.G., Wang, Y.X., Liu, Y., Zou, W., 2020. Wave attenuation by rigid emergent vegetation under combined wave and current flows. Ocean Eng. 213, 107632.
Yin, Z.G., Yang, X.Y., Ma, L., Xu, Y.Z., Lu, H.X., 2016. Numerical investigation on wave attenuation through rigid plants. In: The Second Conference of Global Chinese Scholars on Hydrodynamics. CCSH, China, pp. 448–453.
Zhang, C., Li, Y., Zheng, J.H., Xie, M.X., Shi, J., Wang, G., 2021a. Parametric modelling of nearshore wave reflection. Coast. Eng. 169, 103978.
Zhang, X.X., Lin, P.Z., Nepf, H., 2021b. A simple wave damping model for flexible marsh plants. Limnol. Oceanogr. 66 (12), 4182–4196.

Zhao, Y., Peng, Z., He, Q., Ma, Y.X., 2023. Wave attenuation over combined salt marsh vegetation. Ocean Eng. 267, 113234.
Zhu, L.H., Zou, Q.P., 2017. Three-layer analytical solution for wave attenuation by suspended and nonsuspended vegetation canopy. In: Proceedings of 35th International Conference on Coastal Engineering, vol. 1. ASCE, p. 27.
Zhu, L., Huguenard, K., Zou, Q.P., Fredriksson, D.W., Xie, D., 2020. Aquaculture farms as nature-based coastal protection: random wave attenuation by suspended and submerged canopies. Coast. Eng. 160, 103737.
Zou, Q.P., 2004. A simple model for random wave bottom friction and dissipation. J. Phys. Oceanogr. 34 (6), 1459–1467.
Zou, Q.P., Hay, A.E., 2003. The vertical structure of the wave bottom boundary layer over a sloping bed: theory and field measurements. J. Phys. Oceanogr. 33 (7), 1380–1400.
Zou, Q.P., Peng, Z., 2011. Evolution of wave shape over a low-crested structure. Coast. Eng. 58 (6), 478–488.